Polymer Testing 108 (2022) 107495

Contents lists available at ScienceDirect

Polymer Testing

journal homepage: www.elsevier.com/locate/polytest

Selective dissolution of polysulfone support material of fused filament fabricated Ultem 9085 parts

Ariadna Chueca de Bruijn, Giovanni Gómez-Gras, Marco A. Pérez *

IQS School of Engineering, Universitat Ramon Llull, Via Augusta 390, Barcelona 08017, Spain

ARTICLE INFO

Keywords:
Additive manufacturing
Fused filament fabrication
Support removal
Polysulfone solvent
Ultem 9085
Mechanical performance

ABSTRACT

One of the main advantages of 3D printing lies in the fact that the desired object is constructed layer by layer, enabling the production of complex geometries otherwise unfeasible with conventional manufacturing methods. To create these parts, the use of an auxiliary scaffold structure, made of either the same or a different material than the model, is usually mandatory to avoid structural collapse during fabrication. Such support materials need to be chemically or manually removed after the part is manufactured. However, the removal process can potentially damage the object and poses a problem when the part presents intricate or hidden cavities. This study presents a time-effective, temperature-controlled methodology to dissolve the only commercially available Ultem™9085 (Ultem) support material. The process to select a novel solvent and its effects on Ultem's mechanical performance in terms of compression, tensile and bending properties is addressed. At the same time, the influence of the chemical post-process on Ultem's flammability is evaluated, given that the FST (flame, smoke, and toxicity) certification of this material is one of the most attractive properties for its applicability in certain industrial sectors. Results are supported by optical and scanning electron microscopy. The outcomes of this research are intended to provide practical recommendations for the use and scaling of the proposed solvent by the industrial sector.

1. Introduction

Additive manufacturing technologies have revolutionized the concept of small batch production and end-user customization [1,2]. Particularly, fused filament fabrication (FFF) remains one of the most used and studied additive manufacturing methods to produce prototypes and end-use products for a vast range of applications and industries [3–6]. This fact can be attributed to its operational simplicity, cost-effectiveness compared to similar techniques, and the possibility of working with high-performance and production-grade thermoplastics and its composites [7].

The FFF process, also known as fused deposition modeling (FDM), is based on the construction of physical objects by adding consecutive layers of molten polymeric material, which is extruded in the form of a filament deposited in the printing bed through a heated nozzle. The layered nature of this process enables the construction of complex-shaped parts, unattainable with conventional methods such as subtractive manufacturing [8]. To build overhanging or convex shapes, dual extruder FFF printers use additional material to create scaffolds [9]. After the manufacturing process is completed, the supports must be removed either chemically or manually. Depending on the complexity of the manufactured part, FFF materials' suppliers recommend using either a soluble or break-away support material, the latter being preferred for simpler geometries or the base of the part, as manual extraction with pliers or tweezers can be tedious.

The polyetherimide (PEI) Ultem™ 9085 (Ultem) is an engineering-grade thermoplastic used in FFF with an outstanding chemical and mechanical performance [10–13] that has gained recent interest for its use in the transport and aerospace industries [14]. However, a soluble support material is not yet commercially available. Ultem's high glass-transition temperature (around 180°C) [15] requires a support material with similar thermal properties so that it can be processed in the same heated printing chamber, thus limiting the utilization of other commonly used soluble materials such as polyvinyl alcohol [16,17]. Up to date, the only commercially available support material is a polymeric blend whose main component is polysulfone (PSF), and that needs to be removed mechanically [18].

The chemical structures of PEI and PSF present various similarities. As can be observed in Fig. 1, the chemical structure of both monomeric units contain a diphenyl propane surrounded by an ether group on each side and a high proportion of aromatic rings. These semblances justify their similar thermal stability and chemical resistance to a wide range of organic solvents and diluted acids [19]. Moreover, both

* Corresponding author.
E-mail address: marcoantonio.perez@iqs.url.edu (M.A. Pérez).

https://doi.org/10.1016/j.polymertesting.2022.107495
Received 29 November 2021; Received in revised form 11 January 2022; Accepted 29 January 2022
Available online 16 February 2022

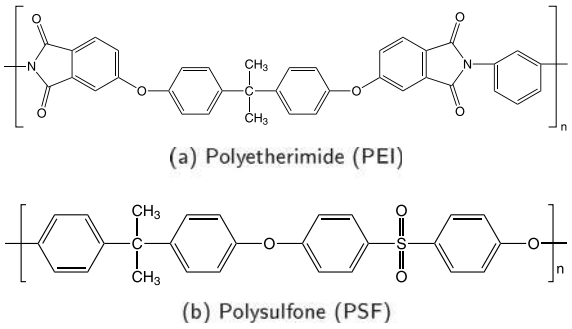

Fig. 1. Chemical structures of the main components of Ultem™ 9085 (PEI) and its support material (PSF).

exhibit poor resistance to halogenated solvents and other substances such as dimethylformamide and N-methyl-2-pyrrolidone [20,21]. Due to its high compatibility, some authors have recently proposed their joint dissolution and further combination to synthesize ultrafiltration membranes to remove soluble azoic dyes [22].

Since there is a growing industrial interest to adopt Ultem as a functional material for FFF parts, new strategies should be developed to successfully and simply remove its support material. To the authors' knowledge, the effect that solvents targeted at the dissolution of PSF have on Ultem's mechanical properties has not been addressed. In a previous contribution made by the authors [23], 1-bromopropane and toluene were preliminarily chosen as proper carrier solvents due to their proven low interaction with Ultem during controlled periods. Nonetheless, considering the aim to escalate the process at industrial levels, toluene should be chosen as a preferred carrier solvent option since the use of halogenated solvents (such as 1-bromopropane) ought to be avoided due to their proven linkage with the greenhouse effect [24]. Regarding the other component of the proposed binary mixture, 1,4-dioxane was previously identified as a potential solubilizer for PSF. However, the presence of redeposited material after the immersion of an Ultem part (without PSF) suggested the partial dissolution of the model material, which supposedly remains unaffected. Despite not resulting in a highly detrimental effect on Ultem's mechanical properties, this dissolution, together with the fact that PSF did not completely dissolve after 4 h of treatment, motivated the research of other alternative solvents.

In this regard, according to the consulted literature, aniline was reported to dissolve PSF during the synthesis of ionic conductive polysulfone composite membranes [25]. Unlike other proposed solvent candidates [23,26,27], aniline presents a significant potential to be used for the selective dissolution of PSF. Furthermore, aniline's miscibility with toluene enables their combined use.

Accordingly, this work aims to present and experimentally validate an optimized procedure for the dissolution of the PSF support material, minimizing the treatment time and the affectation of Ultem's mechanical performance using aniline and toluene. To this purpose, first, the choice of appropriate solvent composition and operational procedure are supported by multiple laboratory analyses, including solubility tests, infrared spectroscopy, viscosity measurements, flammability tests, and through the evaluation of the compressive behavior of chemically treated Ultem cellular solids with intricate shapes. Finally, the proposed procedure is verified via the mechanical characterization of the treated model material under tensile and bending test conditions.

2. Methodology

The approached methodology for the development of the present work can be summarized in three main phases, as depicted in Fig. 2.

Aniline is a well-suited candidate for the dissolution of PSF since pre-study experiments revealed a non-significant visual affectation of

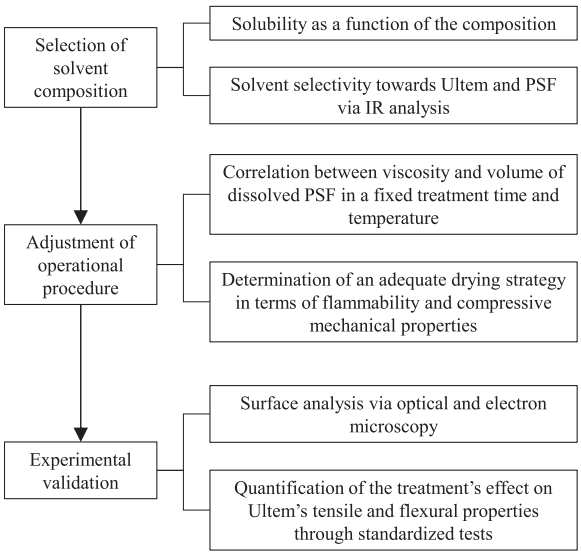

Fig. 2. Schematic of the methodology followed during the development of the present study.

Ultem's surface when it was exposed to aniline for controlled periods. Thus, the first phase consisted of choosing an adequate solvent composition according to the solvent's capacity to dissolve PSF selectively. For that, the solubility of PSF in different dissolutions containing variable volume percentages of aniline in toluene was assessed by fixing a solution volume and gradually dissolving controlled quantities of PSF until saturation. This experiment was performed at ambient laboratory conditions and using a magnetic stirrer to aid in the dissolution process.

To obtain additional information on the kinetics of the dissolution process emulating real process conditions, a second experiment was performed introducing Ultem samples with complex geometries and equal volumes of PSF as support material in equal volumes of solvent mixtures containing different aniline percentages and recording the time needed to achieve complete dissolution. It is worth noting that the process conditions of this test included the use of an ultrasonically agitated and refrigerated water bath with a constant media temperature in the range of 0 to 2°C. This choice was determined by the fact that some sort of agitation method is recommended by FFF manufacturers during the support removal stage of soluble support materials to facilitate the dissolution or detachment of support remains [28]. In this context, ultrasonic agitation often provides a more homogeneous result in comparison to conventional (mechanical) agitation. However, it presents the challenge of overheating of the sonication media during long agitation periods if the agitation equipment is not provided with a temperature control system. In the present case, the temperature rise associated with the agitation process resulted in unacceptable damage of the Ultem parts. Therefore, the use of a cooling system based on the continuous supply of crushed ice, as well as the permanent control of the temperature of the media was key to ensure a desirable dissolution of the PSF while keeping Ultem's integrity.

Aniline's selectivity towards Ultem and PSF was evaluated via attenuated total reflectance Fourier transform infrared spectroscopy (ATR-FTIR), analyzing the composition of the remaining liquid after introducing a fixed mass of both materials in solutions containing variable aniline percentages during a fixed immersion time.

Once the optimal composition was identified, a second phase consisted in determining additional operational process parameters, such as the recommended volume of solvent required to obtain complete PSF dissolution in a fixed treatment time and temperature. In this regard, in a previous contribution on the topic [23] 4 h were needed to achieve almost complete PSF dissolution. Since the herein presented solution

aims to be more time-effective, half of this time, namely 2 h, was chosen as the maximum.

Because the viscosity of the PSF/aniline/toluene system is expected to increase as a function of the amount of dissolved PSF, the kinematic viscosity was chosen as a quantitative and reliable measure to control the PSF content in the mixture. The creation of a calibration curve could, in addition, help to understand if the solvent can be reused to achieve the dissolution of another part's support within the expected time range.

The next studied step of the operational process consisted in determining a suitable drying strategy for treated samples. Given the toxicity of both toluene and aniline and their limited exposure ranges in certain industrial environments [29,30], the need to completely dry Ultem samples after the chemical treatment was considered essential. According to the consulted literature [31,32], vapor pressures of pure toluene and aniline at 25°C are 37 and 0.8 mbar, respectively. These values were used to identify a pressure range needed to evaporate the superficial residues of the solvents in a vacuum chamber.

In this regard, the effect of drying of samples in different pressurized environments was discussed, firstly, in terms of Ultem's flammability to evaluate if it preserved its self-extinguishing capacity after the treatment and, secondly, in terms of compressive mechanical performance of chemically treated and dried Ultem cubic cells with complex geometries. According to the manufacturers, Ultem complies with the regulation 14 CFR 25.853 (a), Appendix F, Part I, Paragraph (a) (1) (ii), regarding the time it takes to self-extinguish a flame applied vertically at a certain distance for fixed periods. Nonetheless, this standard was dismissed as it uses sections of parts of the aircraft components on a real scale, and the present research does not aim to provide indications for a specific component. Therefore, it was decided to follow the UL-94V flame test standard procedure [33], which uses normalized test specimens and allows a similar classification to the previously mentioned standard.

Finally, a third phase was aimed at the experimental validation of the proposed post-process by quantifying the treatment's effect on Ultem's tensile and bending performance and corroboration of the results through surface analysis of scanning electron micrographs.

3. Experimental procedure

3.1. Materials and solvents

The model material for the fabrication of the parts used in the present investigation is PEI Ultem, and the selected support material is PSF. A Stratasys Fortus 400mc professional FFF printer was used to fabricate all samples using the printing settings detailed in Table 1. The PSF used for the solubility and viscosity tests was obtained using break-away support material from previous printing jobs to emulate the morphology of a real-case scenario.

Cubic cellular solids used in solvent optimization and compression tests were designed using nTopology, a design and simulation software for geometry optimization that allows the creation of complex structures using sets of predefined cells. $20 \times 20 \times 20$ mm^3 solid cubes were modified to contain single unit Gyroid or Diamond cells as depicted in Fig. 3. The choice of these unit cells was made due to the possibility to print them with and without support scaffolds. The thickness of the cell walls was fixed at 1.524 mm (the equivalent of two single contours without infill). Nonetheless, in some compression tests, a thicker cell wall (4.572 mm) was used to explore the effect of the wall thickness and infill pattern on the mechanical performance after the chemical treatment.

Regarding solvents, aniline and toluene were used with purity grades higher than 99.5%. Their respective chemical structures are presented in Fig. 4.

Table 1
Summary of the printing process parameters.

Part orientation	X-Flat
Part interior style	Solid*
Support style	Sparse
Infill raster angle	±45°
Model and support tips	T16
Slice height	0.254 mm
Number of contours	1
Contour width	0.508 mm
Chamber temperature	195°C
Model material extruder temperature	380°C
Support material extruder temperature	421°C

*To study the effect of the chemical treatment on different infill configurations and wall thicknesses, some parts for compression tests were fabricated using a model material sparse configuration with a 0.5 mm raster air gap. Others were printed without part interior style as the wall had the thickness of two contour filaments.

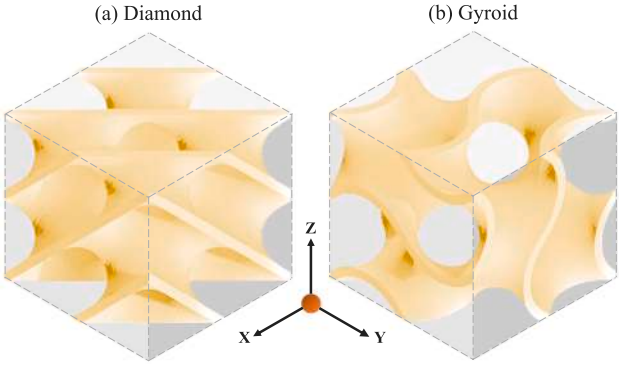

Fig. 3. Schematic of the cellular solids selected for the study: Diamond (a) and Gyroid (b).

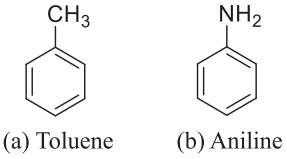

Fig. 4. Chemical structures of toluene (a) and aniline (b).

3.2. Solubility and infrared spectroscopy analysis

The first experiment performed to assess the most adequate solvent composition was the study of PSF's solubility in different dissolutions of aniline in toluene, fixing a solution volume of 30 mL and gradually dissolving controlled quantities of PSF until saturation.

Secondly, FFF Ultem Gyroid cubes containing an approximate PSF support volume of 2 cm^3 were introduced in glass beakers containing 70 mL of solvent mixtures with different aniline percentages, and the time needed to achieve complete dissolution using a low-temperature (0–2°C) ultrasonic agitation system was recorded.

To investigate the solvent's selectivity towards Ultem and PSF, a fixed mass of both materials was introduced in solutions containing 20 and 50% of aniline, respectively, and the composition of the remaining liquid after an immersion time of 2 h was analyzed by ATR-FTIR (previous partial evaporation of the solvent to facilitate the detection of dissolved polymer). Powdered forms of extruded Ultem and PSF were also analyzed using this technique for comparative purposes. The experiments were conducted using a Thermo Fisher Scientific Nicolet™iS™10 infrared spectrometer. ATR-FTIR, in transmittance mode, were obtained using a scanning resolution of 1 cm^{-1} in the range of wavenumbers from 800 to 2400 cm^{-1}. Spectra were examined using OMNIC™Spectra. As identified in the previously published work [23], a

sharp, high-intensity peak at 1720 ±30 cm^{-1} corresponds to the stretching vibration of the carbonyl group (C=O) present in polyetherimides and was chosen as Ultem's characteristic peak. Two double peaks at 1140 ±20 cm^{-1} and 1325 ±25 cm^{-1}, corresponding to the symmetric and asymmetric stretching of the sulfoxide group (S=O), were selected for the identification of PSF.

3.3. Determination of the optimal PSF/solvent ratio

Ultem cellular solids with the same cell geometry but different size and number of cells were submerged in equal volumes of solvent, and the time needed for the complete dissolution of PSF, recorded. The volume was then adapted until the PSF contained in all cases dissolved under 2 h. Following this methodology, an approximate correlation between the amount of PSF and the volume of solvent was found.

The relationship between the viscosity of the solvent-PSF system and the amount of dissolved PSF was studied through the dissolution of controlled amounts of PSF and the subsequent measurement of the kinematic viscosity using an Ubbelohde capillary viscometer (measuring temperature of 25°C).

3.4. Samples drying method

The effect of three drying methods (air drying, drying in a vacuum chamber at 30 mbar for 12 h, and drying in a vacuum chamber at 0.5 mbar for 12 h) was examined through two different analyses: flammability and compression testing.

3.4.1. Flammability testing

To conduct the flammability tests, 3 sets of five rectangular-shaped Ultem specimens of 127.0 × 12.7 × 3.2 mm^3 were chemically treated for 2 h to remove the PSF support base, dried using each of the three selected drying methods, and tested according to the standard's specifications. PSF was manually removed (break-away method) in another set of specimens, while the final set was directly printed without support as a control set. To perform the tests, specimens were vertically mounted and placed above a Bunsen burner tube. A blue 1.9 cm high flame was applied to the center of the lower edge of the specimen for two periods of 10 s separated by a 30 s interval. The individual flame time and the presence of drip particles that ignite were recorded for each test.

3.4.2. Compressive behavior

Compressive tests were performed using a ZwickRoell Z030 universal testing machine equipped with a load cell of 30 kN. Recommendations from the ASTM C365 standard [34] were followed with a crosshead rate of 3 mm min^{-1}. Tests were conducted until the specimens fractured. Values of maximum supported load and stiffness were reported. For each studied drying conditions, wall thicknesses and geometries (summarized in Table 2), five specimens were tested in the in-plane *y*-direction (parallel to the layer deposition direction), and five in the out-of-plane *z*-direction (perpendicular to the layer deposition direction). A total of 200 cellular solid cubes with an equivalent volume of 20 × 20 × 20 mm^3 each were manufactured. It should be noted that the dried specimens were first chemically treated for a period enough to dissolve their support material using the previously identified optimal solvent composition.

3.5. Microscope imaging

A JEOL JSM-6460 scanning electron microscope and an Olympus DSX1000 high-resolution digital microscope fitted with a DSX10-SXLOB1X lens (total magnification: 20X) were used to study the surface morphology of pristine and chemically treated specimens. Due to the non-conductive nature of Ultem, samples were gold-sputtered using a sputter coater prior to scanning electron microscopy (SEM) imaging. For the collection of SEM micrographs, a backscattered electron detector, an accelerating voltage of 10 kV, a spot size of 50 nm, and a working distance of 9 to 10 mm were selected.

Table 2
Geometries and drying methods studied in the compression tests.

Evaluated geometries			
Cell geometry	Wall thickness	Infill pattern	Air gap
Gyroid	1.5 mm	–	-
	4.5 mm	±45° solid	0.0 mm
	4.5 mm	±45° sparse	0.5 mm
Diamond	1.5 mm	–	-

Evaluated drying methods			
Non-dried		Air dried	Vacuum chamber-dried for 12 h
Printed without support	Break-away removal		30 mbar 0.5 mbar

3.6. Tensile and bending tests

The effect of the selected solvent candidate on Ultem's mechanical properties under tensile and bending stresses was studied by chemically treating standardized tensile and bending specimens (printed without support) for 2 h.

The mechanical properties in terms of tensile modulus, tensile strength, and strain at tensile strength were determined accordingly to the ASTM D638 [35] standard (type IV specimens with a thickness of 4 mm) using a ZwickRoell Z030 universal testing machine, equipped with a load cell of 30 kN, and a MTS 634.12F-54 lineal extensometer with a nominal length of 25 mm.

In the case of flexural properties, specimens having a cross-sectional area of 4 × 10 mm^2 and a length of 127 mm were tested following the ASTM D790 standard (three-point bending test, procedure A) [36]. The support span was fixed at 64 mm, and tests were executed until a maximum value of flexural stress was reached. Flexural modulus, flexural strength, and strain at flexural strength were reported.

All mechanical tests were conducted with five replicates.

4. Results and discussion

4.1. Solubility of the ternary system PSF/aniline/toluene

Solubility tests were initially performed to identify a saturation point for each concentration to estimate PSF's solubility. Nonetheless, concentrations of aniline equal or superior to 20% showed increased viscosity and dissolution time as the PSF content was increased, but no precipitation or phase separation were observed after adding amounts of PSF higher than the equivalent of 300 g L^{-1}. Instead, a gel-like mix of PSF-solvent was formed. The state of a solution containing 20% of aniline after the solubility test is shown in Fig. 5a. On the contrary, when the aniline content of the solvent mixture was lower than 20%, the solution became cloudy even at concentrations lower than the equivalent of 20 g L^{-1}. Despite the fact that the added PSF softened, two separate phases (a semi-solid and a liquid phase) could be identified. Fig. 5b and c shows the state of a solution containing 10% of aniline during and 30 min after the solubility tests.

The observed behavior of this system resembles a polymer/solvent/nonsolvent ternary system, where PSF is the polymer, aniline the solvent, and toluene, the nonsolvent. In these systems, specific concentrations of their components give a heterogeneous two-phase system, while other concentrations result in a homogeneous system that evolves into a gel state [37]. The practical implications of having such a system are, firstly, that concentrations below 20% v/v aniline in toluene should be avoided and, secondly, that higher concentrations are all capable of dissolving high volumes of the desired polymer. Therefore, the choice of the optimal aniline concentration (above the 20% limit) and the life of the solvent should be determined by other factors, such as the viscosity of the solution or the time needed to dissolve a certain amount of polymer.

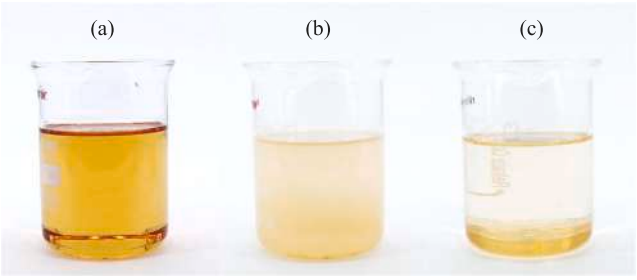

Fig. 5. Representative sample of the state of a 20% to 100% v/v aniline in toluene solution after the PSF solubility tests (a). State of a 10% v/v aniline in toluene solution during (b) and after (c) the solubility tests.

Table 3
Time needed for different concentrations of aniline in toluene to dissolve the PSF of a Gyroid 20 × 20 × 20 mm^3 cube.

Aniline percentage	Testing time[h:min]	Final state of PSF
10	3:10	Not dissolved
20	1:15	Dissolved
30	1:15	Dissolved
40	1:15	Dissolved
50	1:15	Dissolved
60	1:15	Dissolved
70	1:35	Dissolved
80	2:15	Dissolved
90	2:50	Dissolved
100	3:10	Dissolved

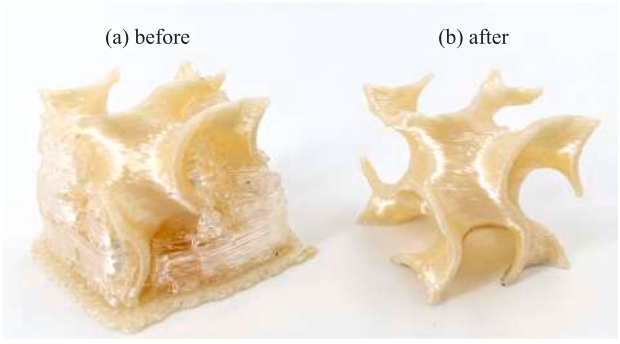

Fig. 6. Gyroid cellular solid before (a) and after (b) the solubility tests.

The time needed to dissolve PSF as a function of the aniline content of the solvent was addressed by submerging ten Gyroid Ultem cubes (printed with an approximate PSF content of 2 cm^3) into ten different solutions containing concentrations of aniline from 10 to 100% in a refrigerated ultrasonic bath. Results of PSF dissolution times are presented in Table 3 and a before and after photography of the test specimens is depicted in Fig. 6. From this experiment, it was found that the dissolving capacity of aniline is enhanced when it is mixed with toluene in certain concentrations (from 20 to 60%) but decreases at higher concentrations as the dissolving time increases. Another finding was that, as reported in Miller-Chou and Koenig [38], polymers do not dissolve instantaneously: the target polymer needs around 40 min to start experiencing changes visible to the naked eye in the form of swelling, followed by a rubbery state and a complete dissolution.

4.2. Solvent selectivity

The ATR-FTIR spectra represented in Fig. 7(a) and (b) show the characteristic peaks of Ultem and PSF, respectively. ATR-FTIR spectra of the remaining liquid of two solutions containing 20 and 50% v/v aniline in toluene after equal masses of Ultem and PSF were submerged

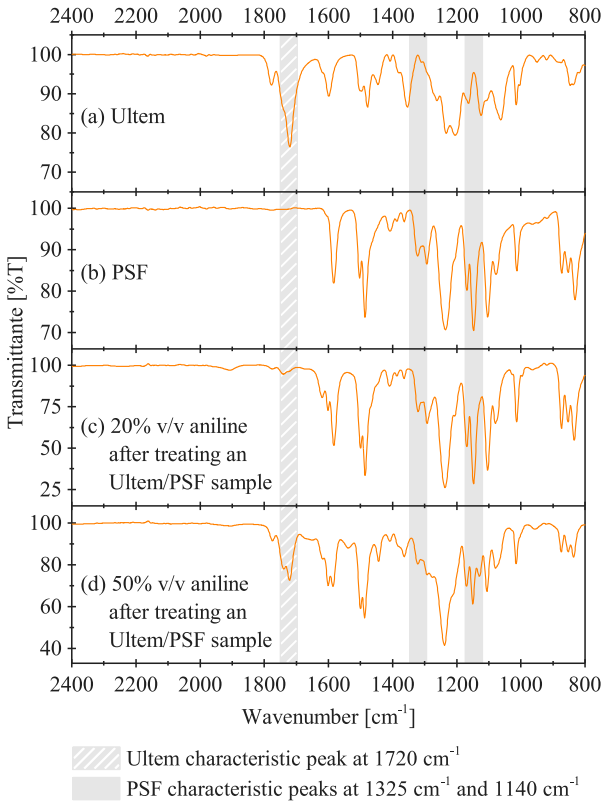

Fig. 7. ATR-FTIR spectra of pulverized Ultem (a) and pulverized PSF (b). Evaporated ATR-FTIR of the remaining liquid from solutions containing a 20% v/v (c) or a 50% v/v (d) aniline in toluene after 2 h of immersion of equal masses of Ultem and PSF.

in them for 2 h (Fig. 6(c) and (d), respectively) show the presence of both Ultem's and PSF's characteristic peaks, which implies the total or partial dissolution of the introduced polymers. Nevertheless, the relative intensity of the Ultem peak in the solution containing a lower concentration of aniline in comparison with the intensity of PSF's peaks is significantly smaller than in the more concentrated solution. In ATR-FTIR, an increase in the peak intensity usually means an increase in the amount (per unit volume) of the functional group associated with the molecular bond. This implies that, although the time needed to dissolve a fixed mass of PSF is the same whether the selected solvent contains 20 or 50% of aniline, Ultem remains less affected in the first case. Adding such phenomena to the higher cost and the higher boiling point of aniline (which hinders its elimination) justifies opting for a final solvent composition containing 20% v/v aniline in toluene. Therefore, this concentration was used in the next steps of the adjustment of the process parameters and in the study of the affectation of the treatment on Ultem's mechanical performance.

4.3. Determination of the optimal PSF/solvent ratio

Taking as a reference the initial solubility tests (see Table 3), 70 mL were needed to fully immerse a 20 × 20 × 20 mm^3 Gyroid cellular solids into the solvent and achieve complete dissolution of its PSF in less than 2 h. Nevertheless, further experiments with bigger cellular solids revealed that the volume of solvent in the first tests was overestimated, as parts containing 25–30 cm^3 of PSF require 275 to 300 mL of solvent for the PSF to be dissolved in less than 2 h. Therefore, the final relationship between the extruded PSF volume and the solvent volume is of 1 cm^3 for every 10 mL, or the required solvent volume to submerge the part, whichever is higher.

The plot in Fig. 8 demonstrates the increase in viscosity as a function of the dissolved volume of PSF filament in 30 mL of solvent. The

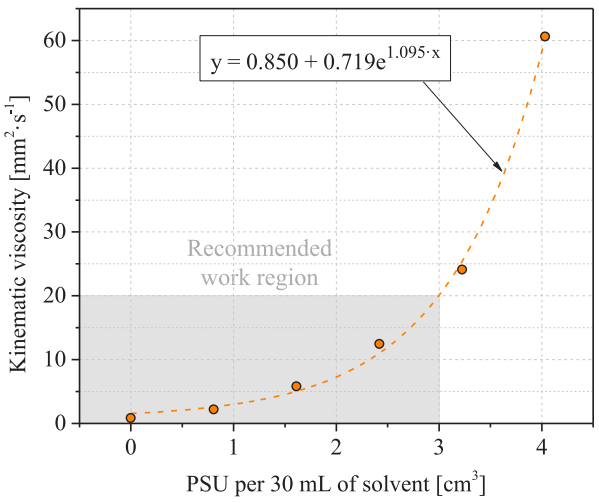

Fig. 8. Kinematic viscosity of the PSF/solvent system at 25°C as a function of the dissolved extruded volume of PSF.

choice of the filament volume as the measuring unit of the amount of dissolved PSF was motivated by the fact that 3D printers provide this information upon processing of the to-be-printed parts. The presented calibration curve was performed by controlling the mass of PSF, which was then converted into the equivalent extruded volume considering a PSF density of 1.24 g cm^{-3}. Since the optimal work region was established at 1 cm^3 of PSF for every 10 mL of solvent (or 3 cm^3 for every 30 mL), the maximum allowed viscosity has been established at 20 mm^2 s^{-1}. Thus, the recommended work region is highlighted in gray in Fig. 8.

4.4. Flammability tests

The time needed for the flaming combustion to be extinguished upon removal of the heat source as a function of the drying method is presented in Fig. 9(a). Results demonstrate that, independently of the used drying method, no specimen burned for more than 3 s after the first or second application of the test flame. Compared with the pristine and vacuum-dried cases, air-dried samples present higher flame extinction time due to flammable solvent residues, which corroborates the need to introduce a drying or cleaning step after the chemical treatment. It should also be noted that the flame extinguishing times for the vacuum-dried samples are similar to the untreated ones and that no detectable differences are observed between the use of a low vacuum (30 mbar) or a high vacuum (0.5 mbar). Furthermore, in addition to not detecting any specimens with persistent glowing combustion after the second removal of the test flame, no flaming drip particles were observed. Fig. 9(b) depicts the final state of the tested specimens as proof that none of them burned up to the holding clamp.

Accordingly, the use of the proposed chemical treatment does not significantly alter Ultem's flame behavior if a drying step is added at the end of the process, thus complying with the UL94V-0 certification.

4.5. Mechanical performance

4.5.1. Compressive behavior

Results on the performance of treated and untreated cellular solids under compressive loads are presented in Fig. 14. The obtained values for stiffness and maximum reached load in the out-of-plane (z) and in-plane (y) directions of chemically treated specimens are presented as percentages of change in comparison to the values obtained for untreated specimens whose support material was mechanically removed. Cellular solids printed without support have also been tested and

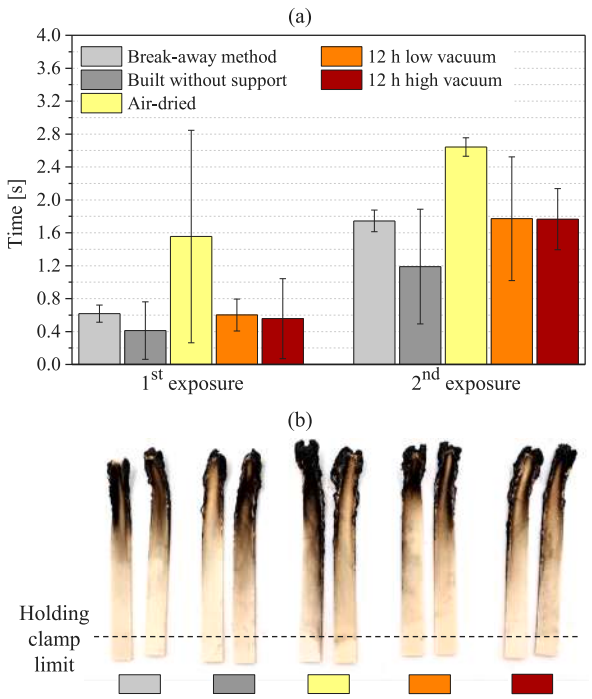

Fig. 9. Results from the flammability tests. Time for the applied flame to be extinguished after the first and second exposures (a). Photographic proof of the state of the Ultem specimens after the tests (b).

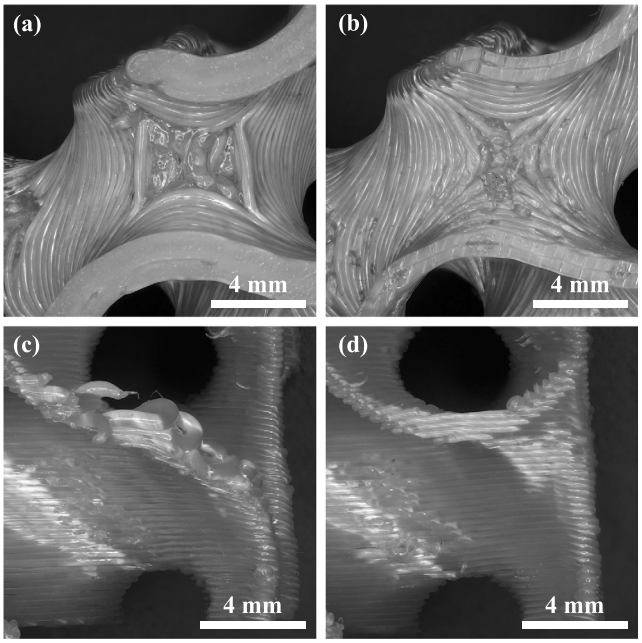

Fig. 10. Optical microscope images showing different finish of the same part printed with support and chemically treated ((b) and (d)) or directly printed without support ((a) and (c)).

included in the comparison. However, it is worth mentioning that, in most cases, it is not possible to avoid the use of support during the manufacturing of complex FFF parts.

An aspect to note is that, when specimens are compressed in the out-of-plane direction (Fig. 14(a–b)), the layers that conform the cellular solid are compacted one against the other, meaning that the layer union plays a minor role compared to when specimens are tested in

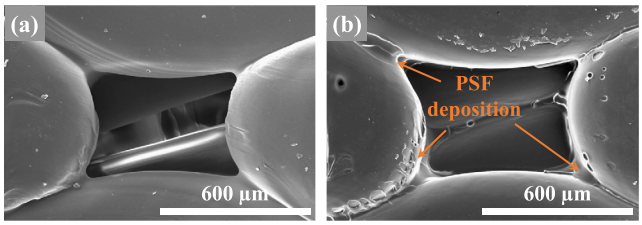

Fig. 11. SEM micrographs of the same region of chemically treated Ultem cellular solids printed without support (a) and printed with support (b).

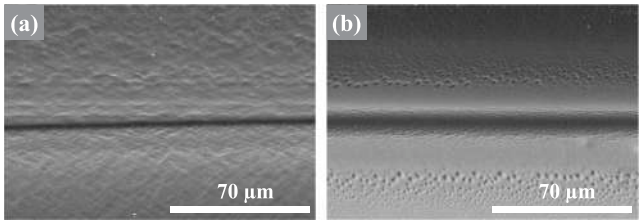

Fig. 12. SEM micrographs of the layer union of Ultem specimens. Images correspond to a pristine sample (a) and a chemically treated sample without the presence of PSF in the media (b).

Table 4
Mechanical properties of pristine and chemically treated Ultem specimens.

	Pristine	Treated	Change
Tensile modulus [MPa]	2436 ±1%	2354 ±2%	−3%
Tensile strength [MPa]	61 ±1%	56 ±4%	−8%
Strain at tensile strength [%]	5.0 ±4%	4.5 ±10%	−10%
Flexural modulus [MPa]	1923 ±5%	1771 ±5%	−8%
Flexural strength [MPa]	85 ±4%	75 ±2%	−11%
Strain at flexural strength [%]	7.6 ±5%	7.2 ±4%	−5%

the in-plane direction (Fig. 14(c–d)). In this last scenario, compressive forces are targeted towards separating the part's layers, creating normal stresses supported by the layer unions.

In terms of compressive properties in the *z*-direction, higher values are obtained when geometries are fabricated without a supporting material compared to the break-away case. An explanation for this lies in how the extruded material is deposited in some areas of the part when no support scaffold is available. In this sense, optical microscope images reveal apparent differences in the finish of parts printed with (Fig. 10(b) and (d)) and without (Fig. 10(a) and (c)) support, which could explain changes in the mechanical properties.

Another point that explains the lower mechanical performance of the specimens with manually removed support material is the weakening of the inter-layer joints during the mechanical removal. In contrast, the observed increase in the chemically treated specimens' stiffness (an average 20% in thinner-walled Gyroid and Diamond geometries and a 12% in the remaining cases) could be explained by the presence of a thin PSF film on the surface of the chemically treated specimens (see Fig. 11) which acts as an adhesive agent that hinders the cellular solid deformation. Besides, these results denote no considerable differences between the different drying methods.

Concerning compressive stiffness in the in-plane direction (y), the no-support printing method results in poorer performance in most cases, demonstrating the need to fabricate parts using support material to enhance inter-layer bonding. Compared to the break-away method, chemically treated parts exhibit a moderately higher stiffness, which can again be explained by the residual support material that has adhered to their walls. Regarding the maximum supported load, no statistically significant differences can be proved between the chemically and the mechanically treated specimens. Despite presenting generally higher average values, the standard deviation of the former group of

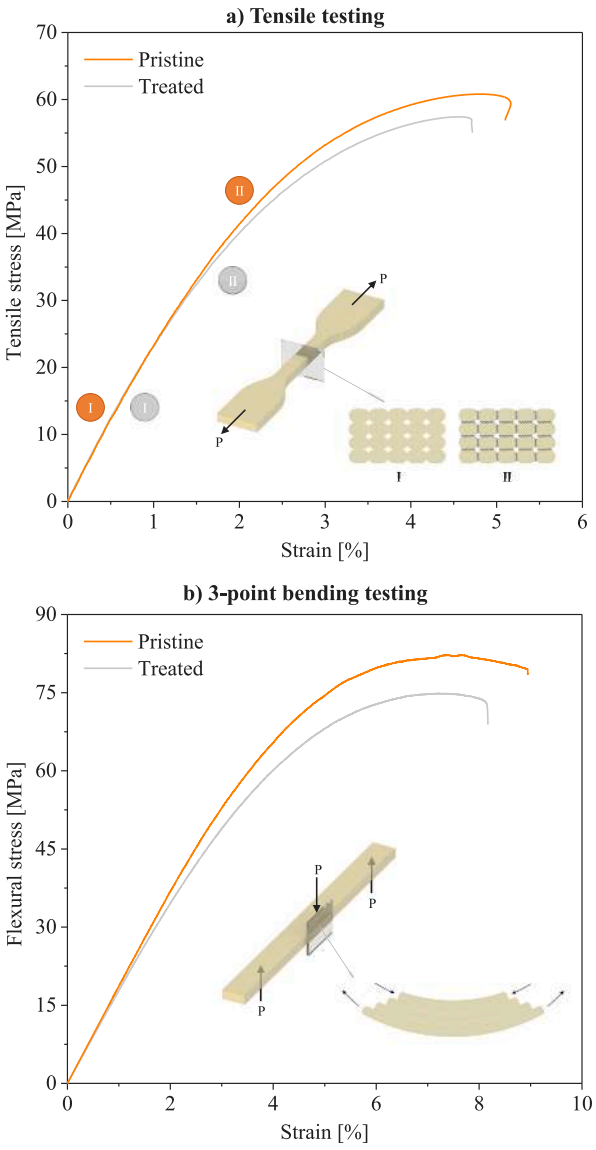

Fig. 13. Representative stress–strain curves showing the chemical treatment's effect on Ultem's response upon tensile (a) and flexural (b) testing.

specimens partially overlaps with the latter group. This means that the degradation of the model material caused by the prolonged contact with the solvent, which has been observed to affect the part's surface adversely (see Fig. 12), is counteracted by the presence of deposited PSF. Both effects result in equal or even lower overall affectation compared to the mechanical damage caused by the manual cleaning of the break-away specimens. Except in the case of the Diamond geometry, the maximum load capacity of specimens printed without support in the in-plane direction falls inside the range of the other studied cases. The fact that this geometry's mechanical performance declines as a result of being manufactured without supports proves once again the need use these auxiliary structures and justifies the importance of the presented work.

4.5.2. Tensile and bending tests

Standard test specimens were treated using the optimal solvent composition and operational procedure and dried in low vacuum conditions for 12 h. No PSF was present in the media to study the worst-case scenario and avoid stiffening and reinforcement of the layer bonding,

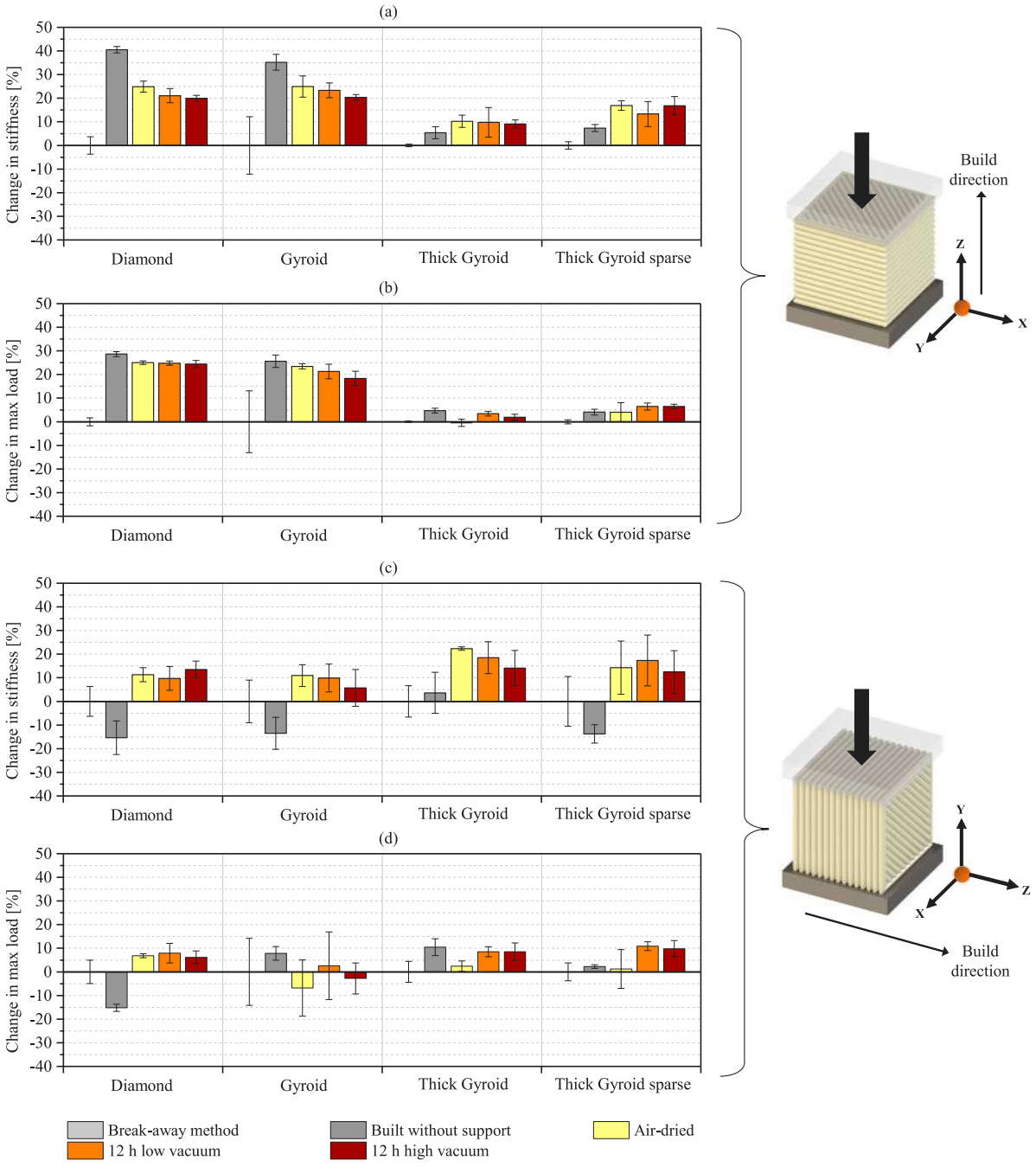

Fig. 14. Average change in the compressive properties (stiffness and maximum reached load) of Ultem cellular solids printed without support or chemically treated and dried using three different methods compared to the manual support removal process.

as demonstrated during compression testing. Fig. 13 shows representative stress–strain curves of reference (untreated) and chemically post-processed Ultem samples under tensile and three-point bending loading conditions. A schematic of the standardized specimens has been added to the plots alongside a graphical representation of the changes undergone by the part's layers as the mechanical tests progress. As demonstrated by the SEM micrographs in Fig. 12, both the outer surface and the layer unions are affected by the presence of a chemical agent. Nonetheless, because unions are usually less mechanically robust, the chemical attack is more damaging to the existent joints between coplanar filaments (intra-layer unions) and adjacent layers (inter-layer unions) than to the filament itself. Additionally, mean values for the obtained tensile and flexural properties of pristine and treated specimens (tensile and flexural moduli, maximum stress, and strain at maximum stress) are displayed in Table 4, alongside the percentage change in these properties.

Overall, results show a moderate decrease in most examined mechanical properties due to Ultem's prolonged contact with the solvent. Most of the changes in properties fall within the experimental error of the tests, which reinforces the feasibility of the proposed support removal method. If longer exposure times are needed due to drastic differences between the geometrical characteristics and support material accessibility of the validated and the real parts, it would be suitable to check that the mechanical performance remains within the expected margins. Tensile modulus and tensile strength have suffered a lesser decrease (3% and 8%, respectively, see Table 4) than the flexural modulus and flexural strength (8% and 11%, respectively). Explanation of this phenomenon lies in the fact that, during a 3-point bending test,

the applied stress is supported by inter-layer unions to prevent sliding of the layers as a result of the shear forces. Since these unions are the most affected region by the solvent, changes are more pronounced than in the tensile test. In this case, the applied stress is more balanced between the filament and the unions during the initial stages of the test (region I in Fig. 13(a)) and supported mainly by the filament at higher strains (region II in Fig. 13(a)). The fact that this second region appears earlier in treated specimens with weakened unions explains the reach of the tensile strength at a slightly lower strain than the pristine case.

5. Conclusions

In this study, an efficient methodology based upon the use of a toluene-based solvent capable of dissolving PSF (Ultem's support material) is presented. Solubility tests and infrared spectroscopy have proven that adding a 20% v/v of aniline to the solvent is beneficial for both the integrity of Ultem and the dissolution of PSF. In addition, kinematic viscosity is found to be a reliable indicator of the amount of dissolved PSF in the liquid media and, as such, a measure of the end of life of the solvent.

In terms of operational procedure, a temperature-controlled, ultrasonicated solution of the proposed solvent can dissolve the equivalent of 1 cm^3 of PSF per 10 mL of solvent under a maximum 2-hours period. Besides, despite not having an influence on the mechanical properties, the use of a vacuum chamber is demonstrated to be necessary to avoid affectation of Ultem's flame extinguishing capacity.

Optical and SEM imaging give insight into the differences observed in the compressive, tensile, and flexural behavior of chemically treated standard specimens compared to pristine counterparts. A thin PSF film between Ultem filaments is considered to be responsible for the enhanced stiffness of compressive specimens. Likewise, a pitting-like chemical attack of the model material (especially in the filament unions) due to the prolonged exposure to the solvent when no PSF is available in the media explains the minor decrease in tensile and flexural strengths.

In short, the proposed approach has proven to be effective in dissolving PSF with reduced impact on the mechanical performance of the model material.

CRediT authorship contribution statement

Ariadna Chueca de Bruijn: Methodology, Validation, Investigation, Writing – original draft. **Giovanni Gómez-Gras:** Conceptualization, Investigation, Writing – review & editing, Formal analysis. **Marco A. Pérez:** Conceptualization, Investigation, Writing – review & editing, Formal analysis, Funding acquisition.

Declaration of competing interest

The authors declare that they have no known competing financial interests or personal relationships that could have appeared to influence the work reported in this paper.

Data availability

The raw data required to reproduce these findings are available to download from Mendeley Data, doi:10.17632/bcd89d2vsm.1. Kindly cite this article and the dataset if utilizing or modifying the data in your work.

Acknowledgments

This work has been supported by the Ministry of Science, Innovation and Universities, Spain through the project New Developments in Lightweight Composite Sandwich Panels with 3D Printed Cores (3DPC) - RTI2018-099754-A-I00. The authors acknowledge nTopology, Inc. for providing educational licenses that enabled the design of the cellular solids. The authors are very grateful to R. Lleida and L. Tiana for the assistance in conducting the experiments.

References

[1] M. Baumers, P. Dickens, C. Tuck, R. Hague, The cost of additive manufacturing: machine productivity, economies of scale and technology-push, Technol. Forecast. Soc. Chang. (ISSN: 0040-1625) 102 (2016) 193–201, http://dx.doi.org/10.1016/J.TECHFORE.2015.02.015.

[2] J. Ding, M. Baumers, E.A. Clark, R.D. Wildman, The economics of additive manufacturing: Towards a general cost model including process failure, Int. J. Prod. Econ. (ISSN: 0925-5273) 237 (2021) 108087, http://dx.doi.org/10.1016/J.IJPE.2021.108087.

[3] S.C. Altıparmak, B. Xiao, A market assessment of additive manufacturing potential for the aerospace industry, J. Manuf. Process. (ISSN: 1526-6125) 68 (2021) 728–738, http://dx.doi.org/10.1016/J.JMAPRO.2021.05.072.

[4] F. Alifui-Segbaya, J. Bowman, A.R. White, R. George, I. Fidan, R.M. Love, Chemical characterization of additively manufactured methacrylates for dental devices, Addit. Manuf. (ISSN: 2214-8604) 31 (2020) 100944, http://dx.doi.org/10.1016/J.ADDMA.2019.100944.

[5] A. Le-Bail, B.C. Maniglia, P. Le-Bail, Recent advances and future perspective in additive manufacturing of foods based on 3D printing, Curr. Opin. Food Sci. (ISSN: 2214-7993) 35 (2020) 54–64, http://dx.doi.org/10.1016/J.COFS.2020.01.009.

[6] A. Mohammed, A. Elshaer, P. Sareh, M. Elsayed, H. Hassanin, Additive manufacturing technologies for drug delivery applications, Int. J. Pharm. (ISSN: 0378-5173) 580 (2020) 119245, http://dx.doi.org/10.1016/J.IJPHARM.2020.119245.

[7] I. Blanco, The use of composite materials in 3D printing, J. Compos. Sci. (ISSN: 2504477X) 4 (2) (2020) 42, http://dx.doi.org/10.3390/JCS4020042, https://www.mdpi.com/2504-477X/4/2/42.

[8] M. Attaran, The rise of 3-D printing: The advantages of additive manufacturing over traditional manufacturing, Bus. Horiz. (ISSN: 0007-6813) 60 (5) (2017) 677–688, http://dx.doi.org/10.1016/J.BUSHOR.2017.05.011.

[9] G. Cicala, D. Giordano, C. Tosto, G. Filippone, A. Recca, I. Blanco, Polylactide (PLA) filaments a biobased solution for additive manufacturing: Correlating rheology and thermomechanical properties with printing quality, Materials (ISSN: 19961944) 11 (7) (2018) 1191, http://dx.doi.org/10.3390/MA11071191, https://www.mdpi.com/1996-1944/11/7/1191.

[10] A. Forés-Garriga, M.A. Pérez, G. Gómez-Gras, G. Reyes-Pozo, Role of infill parameters on the mechanical performance and weight reduction of PEI ultem processed by FFF, Mater. Des. (ISSN: 0264-1275) 193 (2020) 108810, http://dx.doi.org/10.1016/J.MATDES.2020.108810.

[11] K.I. Byberg, A.W. Gebisa, H.G. Lemu, Mechanical properties of ULTEM 9085 material processed by fused deposition modeling, Polym. Test. (ISSN: 0142-9418) 72 (2018) 335–347, http://dx.doi.org/10.1016/J.POLYMERTESTING.2018.10.040.

[12] Y.F. Lv, W. Thomas, R. Chalk, S. Singamneni, Flame retardant polymeric materials for additive manufacturing, Mater. Today Proc. (ISSN: 2214-7853) 33 (2020) 5720–5724, http://dx.doi.org/10.1016/J.MATPR.2020.05.081.

[13] I. Blanco, G. Cicala, G. Ognibene, M. Rapisarda, A. Recca, Thermal properties of polyetherimide/polycarbonate blends for advanced applications, Polym. Degrad. Stab. (ISSN: 0141-3910) 154 (2018) 234–238, http://dx.doi.org/10.1016/J.POLYMDEGRADSTAB.2018.06.011.

[14] J.C. Najmon, S. Raeisi, A. Tovar, Review of additive manufacturing technologies and applications in the aerospace industry, Addit. Manuf. Aerosp. Ind. (2019) 7–31, http://dx.doi.org/10.1016/B978-0-12-814062-8.00002-9.

[15] ULTEM 9085 Production-Grade Thermoplastic for Fortus 3D Printers, Technical Report, Stratasys Inc., 2019, pp. 1–17, URL https://www.stratasys.com/materials/search/ultem9085.

[16] S.J. Park, J.E. Lee, J.H. Park, N.K. Lee, M.Y. Lyu, K. Park, M.S. Koo, S.H. Cho, Y. Son, S.H. Park, Enhanced solubility of the support in an FDM-based 3D printed structure using hydrogen peroxide under ultrasonication, Adv. Mater. Sci. Eng. 2018 (2020) http://dx.doi.org/10.1155/2018/3018761.

[17] C. Duran, V. Subbian, M.T. Giovanetti, J.R. Simkins, F.R. Beyette, Experimental desktop 3D printing using dual extrusion and water-soluble polyvinyl alcohol, Rapid Prototyp. J. (ISSN: 1355-2546) 21 (5) (2015) 528–534, http://dx.doi.org/10.1108/RPJ-09-2014-0117.

[18] SDS ULTEM 9085 Support Material, Technical Report, Stratasys Inc., 2020, URL https://support.stratasys.com/en/materials/fdm/fdm-support-materials.

[19] I.M. Balashova, R.P. Danner, P.S. Puri, J. Larry Duda, Solubility and diffusivity of solvents and nonsolvents in polysulfone and polyetherimide, Ind. Eng. Chem. Res. 40 (14) (2001) 3058–3064, http://dx.doi.org/10.1021/IE001074M.

[20] D. Kyriacos, High-temperature engineering thermoplastics, Brydson's Plast. Mater. Eighth Ed. (2017) 545–615, http://dx.doi.org/10.1016/B978-0-323-35824-8.00021-9.

[21] M.T. DeMeuse, Polysulfones as a reinforcement in high temperature polymer blends, High Temp. Polym. Blends (2014) 165–173, http://dx.doi.org/10.1533/9780857099013.165.

[22] S. Benkhaya, S. M'rabet, R. Hsissou, A.E. Harfi, Synthesis of new low-cost organic ultrafiltration membrane made from polysulfone/polyetherimide blends and its application for soluble azoic dyes removal, J. Mater. Res. Technol. 9 (3) (2020) 4763–4772, http://dx.doi.org/10.1016/J.JMRT.2020.02.102.

[23] A. Chueca de Bruijn, G. Gómez-Gras, M.A. Pérez, Mechanical study on the impact of an effective solvent support-removal methodology for FDM ultem 9085 parts, Polym. Test. (ISSN: 01429418) 85 (December 2019) (2020) 106433, http://dx.doi.org/10.1016/j.polymertesting.2020.106433.

[24] J. Harnisch, D. de Jager, J. Gale, O. Stobbe, Halogenated compounds and climate change, Environ. Sci. Pollut. Res. 2002 96 (ISSN: 1614-7499) 9 (6) (2002) 369–374, http://dx.doi.org/10.1007/BF02987583.

[25] S.I. Voicu, F. Aldea, M. Radut, G. Nechifor, Nanostructured polysulfone composite membranes, U.P.B. Sci. Bull., Ser. B 70 (3) (2008) 39–46.

[26] M. Temtem, T. Casimiro, A. Aguiar-Ricardo, Solvent power and depressurization rate effects in the formation of polysulfone membranes with CO2-assisted phase inversion method, J. Memb. Sci. (ISSN: 0376-7388) 283 (1–2) (2006) 244–252, http://dx.doi.org/10.1016/J.MEMSCI.2006.06.037.

[27] D. Wang, K. Li, S. Sourirajan, W.K. Teo, Phase separation phenomena of polysulfone/solvent/organic nonsolvent and polyethersulfone/solvent/organic nonsolvent systems, J. Appl. Polym. Sci. 50 (10) (1993) 1693–1700, http://dx.doi.org/10.1002/APP.1993.070501003.

[28] Best Practices FDM Support Removal, Technical Report, Stratasys Inc., 2020, URL https://www.stratasys.com/.

[29] M.N. Huda Bhuiyan, H. Kang, J.H. Kim, S. Kim, Y. Kho, K. Choi, Endocrine disruption by several aniline derivatives and related mechanisms in a human adrenal H295R cell line and adult male zebrafish, Ecotoxicol. Environ. Saf. (ISSN: 0147-6513) 180 (2019) 326–332, http://dx.doi.org/10.1016/J.ECOENV.2019.05.003.

[30] L. Huang, H. Cheng, S. Ma, R. He, J. Gong, G. Li, T. An, The exposures and health effects of benzene, toluene and naphthalene for Chinese chefs in multiple cooking styles of kitchens, Environ. Int. (ISSN: 0160-4120) 156 (2021) 106721, http://dx.doi.org/10.1016/J.ENVINT.2021.106721.

[31] M. Al-Lami, D. Havasi, K. Koczka, L.T. Mika, Isobaric vapor–liquid equilibria for binary mixtures of Gamma-valerolactone + toluene, J. Chem. Eng. Data 66 (1) (2020) 568–574, http://dx.doi.org/10.1021/ACS.JCED.0C00791.

[32] S.K. Jangra, J.S. Yadav, N. Dimple, V.K. Sharma, Thermodynamic properties of binary mixtures of tetrahydropyran with anilines at 308.15 K, J. Chem. Eng. Data 55 (10) (2010) 4525–4531, http://dx.doi.org/10.1021/JE1005196.

[33] Tests for Flammability of Plastic Materials for Parts in Devices and Appliances, UL Standard 94, Edition 6, Technical Report, 2013.

[34] ASTM C365 / C365M - 16 standard test method for flatwise compressive properties of sandwich cores, 2016, ASTM Int. West Conshohocken, PA, URL https://www.astm.org/Standards/C365.htm.

[35] ASTM D638-14, Standard test method for tensile properties of plastics, 2014, ASTM Int. West Conshohocken, PA, URL www.astm.org/Standards/D638.

[36] ASTM D790-17, Standard test methods for flexural properties of unreinforced and reinforced plastics and electrical insulating materials, 2017, ASTM Int. West Conshohocken, PA, ISSN 00201685, URL www.astm.org/Standards/D790.

[37] S.-G. Li, T. van den Boomgaard, C.A. Smolders, H. Strathmann, Physical gelation of amorphous polymers in a mixture of solvent and nonsolvent, Macromolecules 29 (6) (1996) 2053–2059, http://dx.doi.org/10.1021/MA9508966.

[38] B.A. Miller-Chou, J.L. Koenig, A review of polymer dissolution, Prog. Polym. Sci. (ISSN: 00796700) 28 (8) (2003) 1223–1270, http://dx.doi.org/10.1016/S0079-6700(03)00045-5.